



Contents lists available at ScienceDirect

Journal of Rock Mechanics and Geotechnical Engineering

journal homepage: www.jrmge.cn

Full Length Article

Application of wave equation theory to improve dynamic cone penetration test for shallow soil characterisation

Miguel Angel Benz Navarrete ^{a,*}, Pierre Breul ^{b,c}, Roland Gourvès ^a^a Sol Solution Géotechnique Réseaux, ZA des Portes de Riom Nord, 23 Avenue Georges Gershwin, Riom Cedex, 63204, France^b Université Clermont Auvergne, Institut Pascal, UMR CNRS 6602, Clermont-Ferrand, 63000, France^c Polytech Clermont-Ferrand Campus des Cézeaux, 2 Avenue Blaise Pascal, Aubière Cedex, 63178, France

ARTICLE INFO

Article history:

Received 27 August 2020

Received in revised form

24 May 2021

Accepted 17 July 2021

Available online 7 September 2021

Keywords:

In situ test

Dynamic cone penetrometer

P.A.N.D.A.

Wave equation

Wave decoupling

Dynamic cone load-penetration (DCLT)

curve

ABSTRACT

Among the geotechnical in situ tests, the dynamic penetration test (DPT) is commonly used around the world. However, DPT remains a rough technique and provides only one failure parameter: blow count or cone resistance. This paper presents an improvement of the dynamic cone penetration test (DCPT) for soil characterisation based on the wave equation theory. Implemented on an instrumented lightweight dynamic penetrometer driving with variable energy, the main process of the test involves the separation and reconstruction of the waves propagating in the rods after each blow and provides a dynamic cone load-penetration (DCLT) curve. An analytical methodology is used to analyse this curve and to estimate additional strength and deformation parameters of the soil: dynamic and pseudo-static cone resistances, deformation modulus and wave velocity. Tests carried out in the laboratory on different specimens (wood, concrete, sand and clay) in an experimental sand pit and in the field demonstrated that the resulting DCLT curve is reproducible, sensitive and reliable to the test conditions (rod length, driving energy, etc.) as well as to the soil properties (nature, density, etc.). Obtained results also showed that the method based on shock polar analysis makes it possible to evaluate mechanical impedance and wave velocity of soils, as demonstrated by the comparisons with cone penetration test (CPT) and shear wave velocity measurements made in the field. This technique improves the method and interpretation of DPT and provides reliable data for shallow foundation design.

© 2022 Institute of Rock and Soil Mechanics, Chinese Academy of Sciences. Production and hosting by Elsevier B.V. This is an open access article under the CC BY-NC-ND license (<http://creativecommons.org/licenses/by-nc-nd/4.0/>).

1. Introduction and state-of-the-art

Among in situ tests, the dynamic probing (ISO-22476-2, 2005) or dynamic penetration test, noted DPT, is the oldest geotechnical characterisation method (Massarch, 2014). DPTs are widely used around the world due to their quick set-up, affordable cost and adaptability to all soil types. However, DPTs provide a single failure parameter: the blow count (N) or the dynamic cone resistance (q_d). This value is not an intrinsic parameter of the soil and its interpretation is still largely empirical.

Indeed, to evaluate dynamic cone resistance, the pile driving formulae are usually employed (Lowery et al., 1968; Sanglerat, 1972; ISO-22476-2, 2005). These are derived from a Newtonian

analysis to relate driving energy and cone penetration to the ultimate strength of the soil. Although the result of the pile driving formulae is a good estimator of the soil strength, application of these expressions presents some theoretical limits (Gonin, 1996, 1999). It is known that penetrometer driving is not a simple problem which can be only solved by Newton's shock theory and nowadays it is well accepted that it is better represented by the wave equation solution.

In fact, Isaacs (1931) and Smith (1960) suggested applying this theory for the study of concrete pile driving, and subsequently many authors worked on the numerical and practical implementation of the wave equation in order to improve the bearing capacity prediction of driven piles (Smith, 1960; Aussedat, 1970; Rausche, 1970; Rausche et al., 1971, 1972, 1985; Meunier, 1974; Goble et al., 1975, 1980; Gonin, 1979, 1996; Middendorp and Weele, 1986; Holeyman, 1992; Hussein and Goble, 2004).

Notwithstanding the analogy with driven piles, few studies have implemented the wave equation solution to improve the interpretation of DPT. In fact, after the first theoretical and practical

* Corresponding author.

E-mail address: mbenz@sol-solution.com (M.A. Benz Navarrete).

Peer review under responsibility of Institute of Rock and Soil Mechanics, Chinese Academy of Sciences.

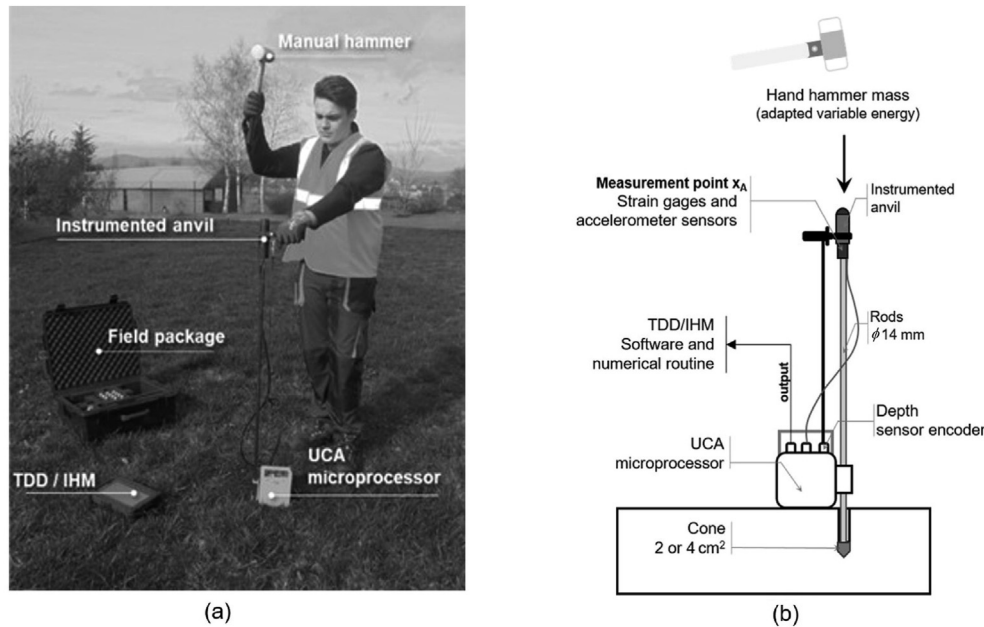


Fig. 1. The P.A.N.D.A. 3 instrumented DPT device (Benz Navarrete, 2009): (a) Field equipment, and (b) General principle and description of instrumented lightweight dynamic penetrometer.

experiments published by Palacios (1977), Schmertmann (1978, 1979), and Schmertmann and Palacios (1979), numerous works were carried out to evaluate energy transmission in standard penetration test (SPT) and obtain the corrected N_{SPT} number for an energy efficiency of 60% (N_{60}) (Seed et al., 1985; Skempton, 1986; Sy and Campanella, 1991; Goble and Aboumatar, 1992, 1994; Aboumatar and Goble, 1997; Butler et al., 1998; Farrar, 1998; Farrar et al., 1998; Batilas et al., 2016).

Among the rare works, Aussedat (1970) in France was certainly the first, by means of a laboratory penetrometer, to obtain stress-strain relation of soil using wave equation and experimental measurements. Later, Chen (1991), Goble and Aboumatar (1992, 1994), and Liang and Sheng (1993) attempted to determine soil parameters with a laboratory instrumented penetrometer in order to improve the pile bearing capacity prediction by wave equation. Nazarian et al. (1998), Kianirad et al. (2011), and Byun and Lee (2013) instrumented lightweight dynamic penetrometers and applied the same approach to correct cone index value by energy transfer and evaluate the soil strength. Recently, Žaržojus et al. (2013) and Kelevisius and Žaržojus (2016) instrumented a dynamic penetrometer super high (DPSH) (ISO-22476-2, 2005) with an accelerometer to improve penetration measurements and blow count.

However, none of these works has made it possible to improve systematically the technology associated with DPT either to implement new methods of measurements and analysis, or to obtain in situ soil stress and strain necessary for the most current geotechnical problems. Although some numerical works on measurement, wave equation interpretation as well as dynamic penetration mechanism in granular media have been published recently (Breul et al., 2009; Escobar Valencia et al., 2013; Quezada et al., 2014; Kotrocz et al., 2016; Poganski et al., 2016, 2017, 2017; Tran et al., 2016, 2017, 2018, 2019; Zhang et al., 2019), these have not also been implemented in practice.

This paper presents the development of a lightweight dynamic penetrometer based on the principle of P.A.N.D.A (Gourvès, 1991; Gourvès and Barjot, 1995; Zhou, 1997), which currently incorporates dynamic measurements, signal processing and wave

equation analysis to continuously provide a dynamic cone load-penetration (DCLT) curve (Benz Navarrete, 2009; Benz Navarrete et al., 2013; Escobar Valencia, 2015; Escobar Valencia et al., 2016a, b). A simple interpretation method of this curve makes it possible to directly estimate additional strain and strength parameters of soils as well as the mechanical impedance and wave velocity of soils by means of the method proposed by Aussedat (1970).

2. Dynamic measurements and wave equation analysis

The P.A.N.D.A., which means *penetrometer autonome numérique dynamique assisté* (from French *pénétrmètre autonome numérique assisté par ordinateur*), is an instrumented lightweight dynamic penetrometer (Gourvès, 1991; Gourvès and Barjot, 1995; Zhou, 1997; Langton, 1999). It is composed of rods with 14 mm in diameter and 500 mm in length and of overflowing conical tips with a cross-section of 2 cm² or 4 cm² (15.9 mm or 22.5 mm in diameter, respectively). According to the standard ISO-22476-2 (2005), the apex angle of cones is 90°. As shown in Fig. 1a, the driving energy is provided manually by means of a hand-hammer mass hitting the instrumented anvil. Driving energy can be thus adapted according to the soil stiffness variations without the measurement being influenced by the impact force or being operator-dependent, since for each blow the energy supplied is directly measured. As per ISO-22476-2 (2005), in the classic version of P.A.N.D.A., the dynamic cone resistance (q_d) is obtained by means of the modified Dutch formula.

A new version of the device was designed by Benz Navarrete (2009), the P.A.N.D.A. 3 (Benz Navarrete et al., 2013; Escobar Valencia, 2015), hereinafter called the instrumented DPT (Fig. 1). It is based on the same functional principle of the device developed by Gourvès (1991), but incorporates new sensors. These are installed on the penetrometer's anvil and used to measure the strain $\epsilon(x, t)$ and acceleration $a(x, t)$ variations caused within the rods by the compressional wave created immediately after each hammer blow. The instrumentation of the anvil is composed of strain gauges with a measurement range of ± 45 kN and installed in a Wheatstone bridge that compensates lateral deformations. The

wave force, $F(t)$, is calculated from the measured strain $\epsilon(x, t)$ using Hooke's law. Miniature piezoresistive high- g shock accelerometers with a measurement range of $\pm 20,000g$ are equally installed close to the strain gauges ($1g = 9.81 \text{ m/s}^2$). A displacement sensor is also installed in the central acquisition unit (UCA, from French *unité centrale d'acquisition*). It is connected to the instrumented anvil to measure simultaneously the cone penetration displacement $s(t)$ per blow (Fig. 1).

The UCA is placed at ground level during the penetration test and continuously records the signals measured by each sensor, which are sampled up to a 250 kHz frequency at 24-bit resolution. Time record per blow is either 100 ms or 200 ms. After each hammer blow, the UCA sends all data to the transfer dialog data (TDD) box which conditions, processes, and stores each measured signal by means of a specially designed software containing the algorithms presented below. The signal processing of raw measurement includes a baseline correction and a signal filtering by means of a low-pass finite impulse response (FIR) filter using a rectangular window and a cut-off frequency of 25 kHz. An example of a measurement recorded during the test is shown in Fig. 2.

From a point of view of the penetrometer driving phenomenon, when the hammer, animated by a speed v_m , strikes the anvil, a compressional wave $u(x, t)$ is generated in the rods and propagates at a constant velocity c towards the cone of the penetrometer. Afterwards, when $u(x, t)$ reaches the cone/soil interface, a part of it is transmitted to the soil, causing its deformation. The second part of the wave is reflected upwards into the rods and travels to the top of the penetrometer, where a new downward wave reflection occurs. The phenomenon becomes thus cyclical during cone penetration.

Considering an elastic rod with both uniform section A_t and length L_t , if external forces (e.g. skin friction) along the rods are negligible, the wave $u(x, t)$ propagation is described by Jean le Rond d'Alembert's equation, known as the wave equation:

$$\frac{\partial^2 u(x, t)}{\partial t^2} = c^2 \frac{\partial^2 u(x, t)}{\partial x^2} \quad (1)$$

Being for the case of the penetrometer a one-dimensional propagation phenomenon and according to the method of

characteristics (Abbott, 1966; Middendorp and Weele, 1986; Verruijt, 2010), the general and most used solution to this equation is given by the overlap of downward $u_f(x-ct)$ and upward $u_g(x+ct)$ waves, where u_f and u_g are the arbitrary respective functions:

$$u(x, t) = u_f(x-ct) + u_g(x+ct) \quad (2)$$

Knowing the u_f and u_g waves at a point x_A in the rods, it is possible to determine for each x point along the rods, the stress $\sigma(x, t)$, strain $\epsilon(x, t)$, velocity $v(x, t)$ as well as displacement $u(x, t)$. In fact, for a plane wave and single mode propagation, stress, strain, velocity, and displacement can be expressed in terms of the Fourier transforms and as a function of these waves:

$$\left. \begin{aligned} \tilde{\epsilon}(x, \omega) &= A(\omega)e^{-i\xi(\omega)x} + B(\omega)e^{i\xi(\omega)x} \\ \tilde{\sigma}(x, \omega) &= E^*(\omega) \left[A(\omega)e^{-i\xi(\omega)x} + B(\omega)e^{i\xi(\omega)x} \right] \\ \tilde{v}(x, \omega) &= -\frac{\omega}{\xi(\omega)} \left[A(\omega)e^{-i\xi(\omega)x} - B(\omega)e^{i\xi(\omega)x} \right] \\ \tilde{u}(x, \omega) &= \frac{i}{\xi(\omega)} \left[A(\omega)e^{-i\xi(\omega)x} - B(\omega)e^{i\xi(\omega)x} \right] \end{aligned} \right\} \quad (3)$$

where $A(\omega)$ and $B(\omega)$ are the Fourier components of the downward u_f and upward u_g waves, respectively; $E^*(\omega)$ is the complex Young's modulus; and ω is the angular frequency. The wave number $\xi(\omega)$ is a complex function defined by $\xi(\omega) = k(\omega) + i\alpha(\omega)$, where k and α are the real and imaginary components. The two parameters, $E^*(\omega)$ and $\xi(\omega)$, depend only on the rod characteristics, geometry and material (Bussac et al., 2002; Lodygowski and Rusinek, 2014; Othman, 2014).

The general problem is thus reduced to determine the Fourier components $A(\omega)$ and $B(\omega)$, which is the same as determining u_f and u_g in the time domain from Eq. (2). In practice, dynamic measurements during penetrometer driving can be performed by means of strain gauges and accelerometers. However, decoupling waves and the assessment of u_f and u_g components are not an easy task. This is because these waves are noisy and often superimposed in recorded signal, especially in the case of a penetrometer where steel and short rods are employed (wave velocity in steel is about 5200 m/s). Therefore, it is necessary to separate them by means of adapted and precise methods.

2.1. Wave decoupling and cone signal reconstruction

Wave decoupling can be performed by different methods. These are distinguished on the types and number of sensors used as well as initial and boundary conditions. Without underestimating the signal processing methods developed during the last 30 years for pile dynamic test (Goble et al., 1980; Hussein and Goble, 2004; Middendorp and Verbeek, 2006), actually, the most precise and effective methods for wave decoupling and waveform calculation have been developed for rapid shocks tests, split Hopkinson pressure bar (SPHB) tests as well as solving percussion problems of rocks (Zhao and Gary, 1997; Park and Zhou, 1999; Bussac et al., 2002; Casem et al., 2003; Jung et al., 2006; Othman, 2014), as shown in Lodygowski and Rusinek (2014).

In the present instrumented DPT, the used method is based on a single x_A point measurement on the rod, at the instrumented anvil, where strain $\epsilon_A(t)$ and acceleration $a_A(t)$ are recorded, from which the velocity $v_A(t)$ is calculated. In the point x_A of measurements, the downward and upward waves are separated from $\epsilon_A(t)$ and $v_A(t)$ recorded signals by

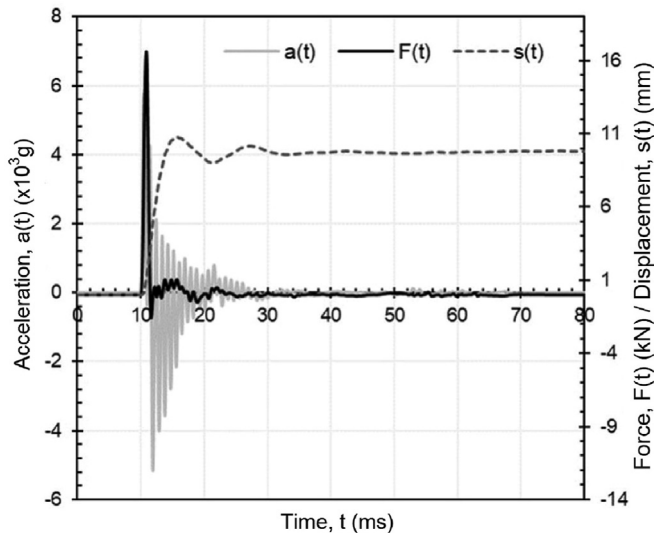


Fig. 2. Example of a raw measurement of force $F(t)$ (black line), acceleration $a(t)$ (grey line) and displacement $s(t)$ (grey dashed line) recorded for one blow during the penetrometer driving.

$$\left. \begin{aligned} \varepsilon_f(x-ct) &= \frac{1}{2}\varepsilon_A(t) - \frac{1}{2c}v_A(t) \\ \varepsilon_g(x+ct) &= \frac{1}{2}\varepsilon_A(t) + \frac{1}{2c}v_A(t) \end{aligned} \right\} \quad (4)$$

where $\varepsilon_f(x-ct)$ and $\varepsilon_g(x+ct)$ are the strains of the downward and upward waves, respectively; $\varepsilon_A(t)$ and $v_A(t)$ are the strain and velocity records at measurement point x_A ; and c is the wave velocity in the steel rods (~ 5200 m/s). Alternatively, the Bussac-Collet-Gary-Othman (BCGO) method (Bussac et al., 2002) can be used to obtain the Fourier components $A(\omega)$ and $B(\omega)$ of Eq. (3) from which and through an inverse Fourier transform $\varepsilon_f(x-ct)$ and $\varepsilon_g(x+ct)$ signals can be finally obtained.

Once the waves $\varepsilon_f(x-ct)$ and $\varepsilon_g(x+ct)$ are separated at measurement point x_A , the next step is to reconstruct the strain, stress, velocity and displacement signals at penetrometer's cone, located at a distance $(x_J - x_A)$ below the measurement point x_A . Assuming that there are neither variation in external forces or mechanical impedance along the rods, the iterative method presented in Eq. (5) and proposed by Lundberg and Henchoz (1977), Karlsson et al. (1989), and Carlsson et al. (1990) is suitable to rebuild stress $\sigma_n(t)$ and velocity $v_n(t)$ for each x_n section along the rods.

$$\left. \begin{aligned} \sigma_n(t) &= \frac{1}{2} \left[\sigma_{n-1}(t + \Delta t_{n-(n-1)}) + \sigma_{n-1}(t - \Delta t_{n-(n-1)}) \right] + \frac{Z_n}{2} \left[v_{n-1}(t + \Delta t_{n-(n-1)}) - v_{n-1}(t - \Delta t_{n-(n-1)}) \right] \\ v_n(t) &= \frac{1}{2} \left[v_{n-1}(t + \Delta t_{n-(n-1)}) + v_{n-1}(t - \Delta t_{n-(n-1)}) \right] + \frac{1}{2Z_n} \left[\sigma_{n-1}(t + \Delta t_{n-(n-1)}) - \sigma_{n-1}(t - \Delta t_{n-(n-1)}) \right] \end{aligned} \right\} \quad (5)$$

where $\Delta t_{n-(n-1)} = (x_{n-1} - x_n)/c$ and $\Delta Z_n = (E_n/c)$, in which Z_n and E_n are the mechanical impedance and Young's modulus at the section n , respectively. As represented in Fig. 3, according to this method, if the geometry and the distance between impedance change planes are known, the stress and velocity at the lower extremity n can be calculated from previous measurement point $(n-1)$ where stress and velocity were known. In Fig. 3, a longitudinal rod having different impedance changes represents the penetrometer. Section A represents the point x_A where strain gauges and accelerometers are installed while the cross-section J (if the skin friction along the rod string is negligible) represents the soil/cone interface, where stress, force, velocity and displacement must be established (Carlsson et al., 1990). Section J is chosen to represent cone/soil interaction because it integrates all forces that the soil exerts on the cone (shaft and base) during penetration per blow. To compute stress, force and velocity for the cone/soil section x_J from the signals recorded at x_A , each

impedance changes along the rod string must be solved in advance.

In the case of the current instrumented DPT, where rods are elastic and homogenous, and considering there are no impedance changes at the connection sections as well as no external skin forces along the rods, the major impedance change takes place at the rod/cone and cone/soil sections (represented by C and J in Fig. 3). Wave attenuation caused by connectors and length of rods is negligible. In fact, it has been largely studied for the SPT and it was estimated that the effects of energy losses in the rod string to depths of up to 30 m were not significant and less than 1.5% (Palacios, 1977; Farrar, 1998; Farrar et al., 1998; Odebrecht et al., 2005). Thus, cone signals are calculated by two iterations of Eq. (5):

- (1) In the first iteration, we calculate the stress $\sigma_C(t)$ and velocity $v_C(t)$ for section C (noted n) (Fig. 3) from $\sigma_A(t)$ and $v_A(t)$ recorded in the measurement section A (noted $n-1$) by using Eq. (5).
- (2) In the second iteration, stress $\sigma_J(t)$ and velocity $v_J(t)$ for section J (noted n) (Fig. 3) are calculated from stress and velocity records that were calculated previously for section C (noted $n-1$).

This method has the advantage of being suitable for a wide

range of impact velocities and the results obtained are theoretically accurate. In addition, there is no limitation for geometry along the rods of the penetrometer if the measurement sensors are installed in a uniform section where the waves are as uniform as possible. Once the stress $\sigma_J(t)$ and velocity $v_J(t)$ signals are calculated for the penetrometer cone, strain $\varepsilon(t)$ and force $F(t)$ are calculated by means of elasticity relationships presented in Eq. (3). Displacement $u_f(t)$ can be also calculated through numerical integration of velocity $v_f(t)$.

An example of raw measurements, force $F(t)$ and velocity $v(t)$, carried out throughout the test and made at the measurement point x_A are presented in Fig. 4a. Here, velocity is multiplied by the mechanical impedance of the rod ($Z = EA/c$, where E is the steel Young's modulus and A is the rod section) to express it in terms of force. From these signals (Fig. 4a) and by applying the presented formulations (Eq. (4)), decoupled forces of the upward and downward waves are obtained (Fig. 4b). Calculated cone signals of

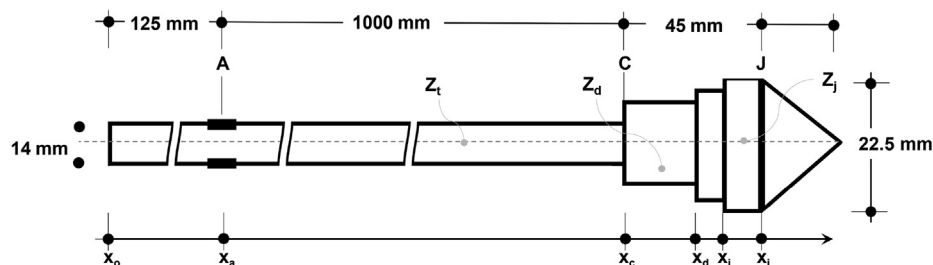


Fig. 3. Diagram of the method for decoupling and rebuilding waves along the penetrometer's rods implemented in the presented instrumented DPT.

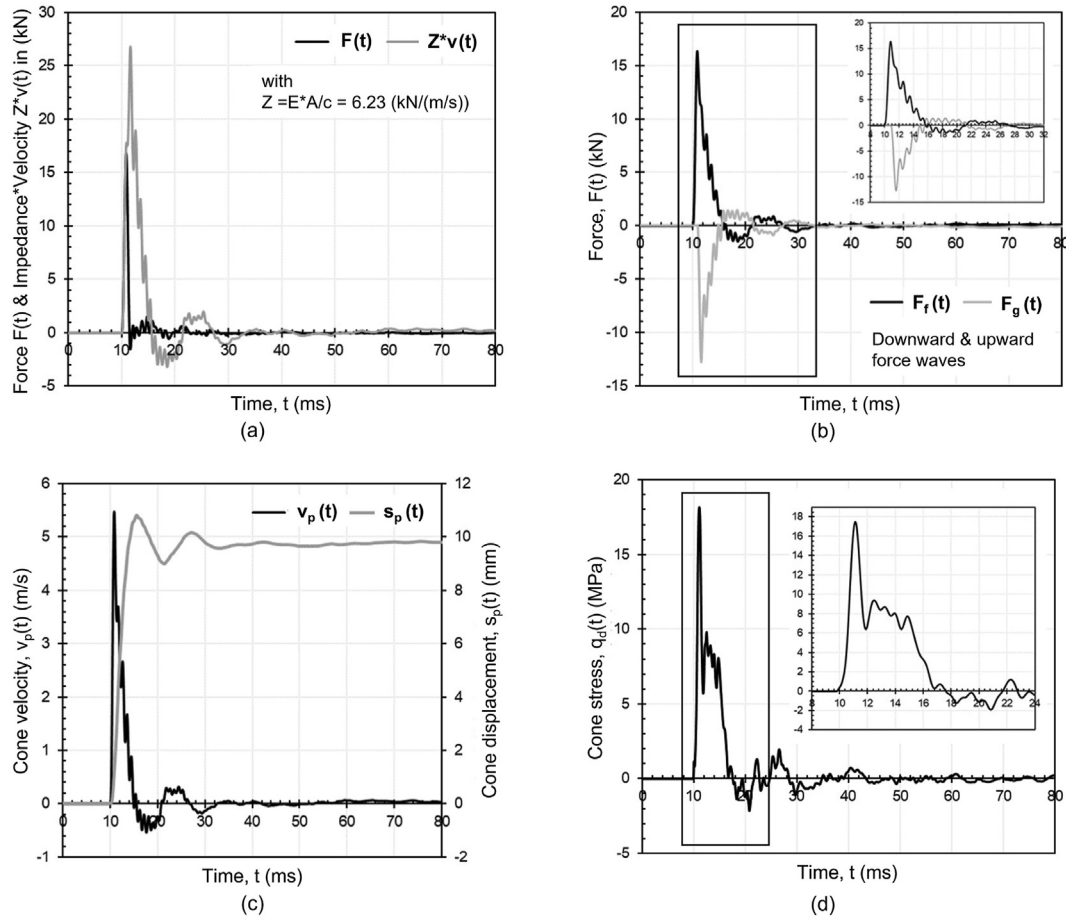


Fig. 4. Example of dynamic measurement during penetrometer driving for Allier sand in a dense state: (a) Signals of force (black line) and velocity (grey line) multiplied by rod mechanical impedance $Z = EA/c$ recorded at the measurement point x_A in the instrumented anvil of the device, (b) Decoupled forces of upward (grey line) and downward (black line) waves travelling into the rods after the blow, (c) Calculated cone signals for velocity $v_p(t)$ (black line) and displacement $s_p(t)$ (grey line), and (d) Calculated stress signal at the cone of the penetrometer with a zoom view between 8 ms and 24 ms.

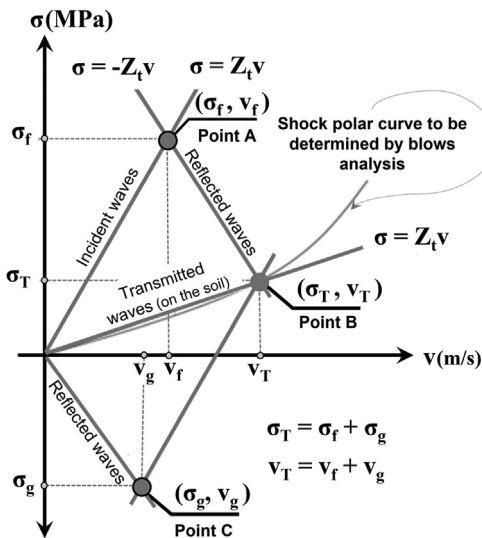


Fig. 5. Diagram of the principle of the shock polar method (after Aussedat, 1970).

velocity $v_p(t)$, displacement $s_p(t)$ and total soil resistance $q_d(t)$, obtained using Eq. (5), are also presented. The calculated velocity $v_p(t)$ as well as displacement $s_p(t)$ of the cone is presented

simultaneously in Fig. 4c. The stress $q_d(t)$ mobilised during the cone penetration at the cone/soil interface is presented in Fig. 4d. In addition, assuming that there is equal stress and displacement at the cone/soil interface during cone penetration, it is possible to plot the DCLT curve. Theoretical, numerical as well as practical reliability of these method has been demonstrated recently by Benz Navarrete et al. (2013), Escobar Valencia et al. (2013, 2016a, b), Tran et al. (2017, 2019), and Zhang et al. (2019).

2.2. Assessment of soil mechanical impedance, wave velocity and strain using shock polar curves

To assess soil mechanical impedance, wave velocity as well as strain, the shock polar curve method is applied (Aussedat, 1970; Meunier, 1974; Oularbi, 1989; Oularbi and Levacher, 2009; Lodygowski and Rusinek, 2014; Omidvar et al., 2014; Iskander et al., 2015; Tran et al., 2019). As shown in Fig. 5, the polar shock curve represents the relationship between stress (σ) and particular velocity (v) generated by the mechanical wave which propagates in a defined material. In this method, it is assumed that a plane and unidirectional elastic shock wave propagates from a medium A (rods) to a medium B (soil). Both media have different mechanical impedances, and in our case, the mechanical impedance of the rods is greater than that of the soil. The main purpose here is to obtain the soil shock polar curve from decoupled waves in the measurement section x_A of the penetrometer, close to the anvil.

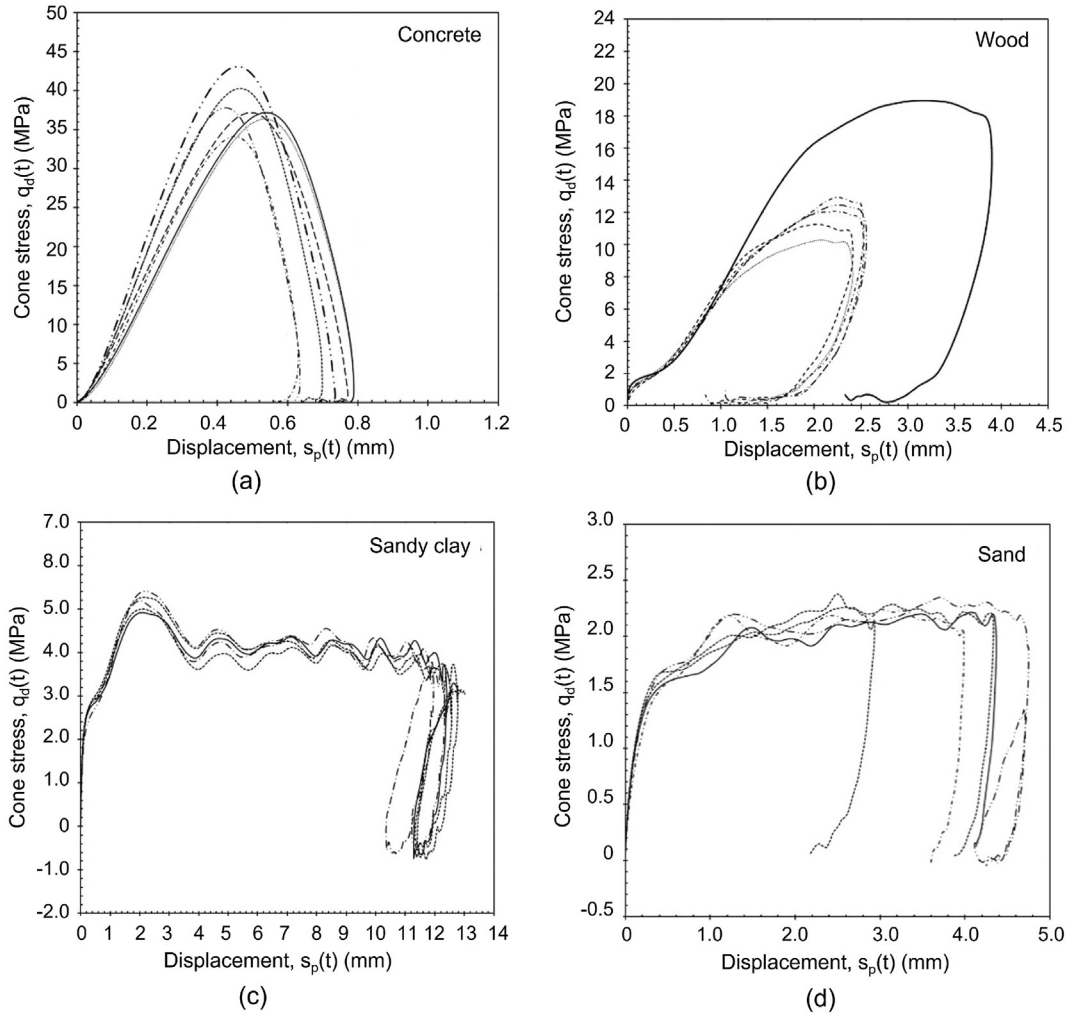


Fig. 6. DCLT curves obtained from decoupled waves and cone signal calculation method on (a) concrete, (b) wood, (c) sandy clay and (d) sand. For each graph, each curve represents an analysed blow.

Considering the penetrometer and the soil at rest, just after the blow, the penetrometer rods are crossed by the compression incident wave $u_f(t)$. After its passage, the relationship between the stress σ_f and particular velocity v_f can be expressed according to Eq. (6), which is represented by the grey straight line with a slope positive of Z_t (Fig. 5). When the incident wave reaches the soil/cone interface, a transmitted wave $u_T(t)$ into the soil occurs while a reflected wave $u_g(t)$ is returned upwards into the rods. The stress resulting after its passage can be expressed as

$$\sigma_f = \frac{E}{C} v_f = \rho C v_f \quad (6)$$

$$\sigma_g = -\frac{E}{C} v_g = -\rho C v_g \quad (7)$$

The pair of points A (σ_f , v_f) and C (σ_g , v_g) in Fig. 5 belong to the rod polar shock curve defined by the slope $Z = \pm \rho c$, where ρ is the density of the steel rod. In the soil, immediately after the passage of the transmitted wave $u_T(t)$, the stress σ_T as well as the particular velocity v_T increases proportionally (Eq. (8)). At the soil/cone interface, the incident and reflected wave overlap and resulting stress σ_T and particular velocity v_T can be expressed as a function of these waves according to Eqs. (9) and (10). Thus, the point B (σ_T , v_T) belongs to the soil polar shock curve (Fig. 5). In Fig. 5, black straight

line represents the rod polar curve, characterised by its mechanical impedance Z_t (defined from the material properties), the Young's modulus E (2.1×10^{11} Pa in our case) and the wave velocity c (~ 5200 m/s). The grey dashed curve represents the soil shock polar curve, intercepting the polar curve of the rods at point B where the stress and velocity of incident, reflected and transmitted waves converge. Once this point is identified, the shock polar curve of the soil and consequently its mechanical impedance Z_s can be determined.

$$\sigma_T = \frac{E_s}{C_s} v_T = \rho_s C_s v_T \quad (8)$$

$$\sigma_T = \sigma_f - \sigma_g \quad (9)$$

$$v_T = v_f + v_g \quad (10)$$

According to Fig. 5, for the case of steel penetrometer rods, the polar shock curve is a straight line defined by the slope $Z = \pm \rho c$; while for the soil, the shape of this curve remains unknown and must be determined experimentally. In practice, a part of soil polar shock curve can be obtained from penetrometer measurements and for the time interval $t_0 + 2L/c$ as follows, where t_0 is the trigger time and L is the rod length:

- (1) Consider decoupled incident and reflected waves (Eq. (4));
- (2) Compute stress and velocity for incident and reflected waves (Eq. (6) and (7));
- (3) Compute stress and velocity of transmitted wave (Eq. (9) and (10)); and
- (4) Plot transmitted stress σ_T as a function of velocity v_T and fitting the curve $\sigma_T = Z_s v_T$.

Furthermore, knowing the impedance of the soil Z_s and considering the short load rise time of wave during the first arrival of the wave-front at the soil-cone interface (less than 400 μ s, as shown in Fig. 4), it can be accepted that the soil behaviour is almost elastic, and it has no time to deform radially. The deformation during this short time is mainly axial and thus it is possible to assess the soil compressional wave velocity c_p and the strain ϵ_{xx} by

$$c_p = \frac{Z_s}{\rho_s} \quad (11)$$

$$\epsilon_{xx} = \frac{v_T}{c_s} \quad (12)$$

Nevertheless, in the practical case of in situ soil characterisation and if the penetrometer driving energy is high, it is important to note that the value of compressional wave velocity (Eq. (11)) determined through this method can be affected by the presence of the groundwater table. In all cases, the soil under dynamic compression loading will behave in undrained condition, which means that its Poisson's ratio will be close to 0.5, especially for the first wave-front arrival (Verruijt, 2010). In such cases, the values obtained should be carefully considered.

3. DCLT curve: Proof of concept

3.1. Experiments on different materials: Sensitivity and repeatability tests

The first experiments conducted aim to determine the DCLT curve for different materials: wood, concrete, sand and sandy clay (Fig. 6). The main purposes of these experiences are to evaluate the repeatability and the sensitivity of DCLT curves obtained with a simplified test configuration. In addition, it aims to assess whether Aussedat (1970)'s method can be used to determine the mechanical impedance as well as wave velocity of soil.

For wood, concrete and sand, the tests were performed in laboratory with variable driving energy using a 1726-g hand hammer. The wood measurements (Douglas fir) were carried out parallel to the fiber direction on a sample with dimensions of 500 mm \times 300 mm \times 180 mm. For concrete, the measurements were performed directly on a 240-mm thickness slab; while the sand sample was prepared and compacted in a cylindrical mould with a diameter of 160 mm and a height of 320 mm. The height of each sample was adapted in order to avoid, as much as possible, the effect of the bottom reflection on the first reflection wave coming from the cone/sample interface, as proposed by Aussedat (1970). For measurement on sand as well as wood and concrete samples, variable driving energy was used.

To evaluate the repeatability and accuracy of this method, the tests performed on the natural sandy clay were carried out at a constant driving energy, by dropping a hammer from a constant height (hammer mass of 5 kg and a fall height of 500 mm). For this purpose, a classic DPT driving system was adapted to the device and a 4-cm² cone section was employed to avoid any skin friction along the rods.

All the tests were carried out with two assembled rods of 14 mm in diameter and 500 mm in length (total length of rod was

1000 mm). The rods were strongly screwed together without any specific connection element that could generate modification of the waves that propagate inside them. For each material, at least five blows were recorded and analysed.

DCLT curves obtained for a series of recorded blows on each sample are presented in Fig. 6. Firstly, the good repeatability of curves obtained can be observed as well as its sensitivity to the type of material tested: concrete, wood, sandy clay and sand. Indeed, DCLT curves obtained for concrete and wood (Fig. 6a and b) show a good agreement with those reported for similar tests in the literature (split Hopkinson pressure bar (SHPB), static indentation hardness test, etc.) (Ross et al., 1986; Widehammar, 2004; Lodygowski and Rusinek, 2014; Omidvar et al., 2014, 2015; Iskander et al., 2015). Additionally, from the results obtained for natural sandy clay, performed with a constant driving energy, a very good repeatability can be observed (Fig. 6c). In this case, the curves obtained are almost identical for each blow.

Concerning the curves obtained for sand at variable driving energy (Fig. 6d), it can be noted that the cone load increases proportionally to the displacement, following a nonlinear trend, as usually observed on base load-displacement response of piles in sand. It can also be observed that a maximum soil penetration resistance remains almost constant for each blow independently of driving energy, while total penetration increases proportionally. In addition, for driving energy employed here to obtain sand's DCLT curves, no significant rate effects on cone resistance were observed in our experiences, such as found in other similar experimental cases (Eiksund and Nordal, 1996).

For the case of soils, once cone resistance $q_d(t)$ reaches a threshold value (close to the maximum stress), the soil deforms plastically and the cone resistance $q_d(t)$ remains almost constant until the maximum penetration is reached. At this moment, the energy contained in the waves propagating inside the rods is not enough to continue deforming the soil and the unloading phase begins. After, a series of unloading and reloading cycles can be observed in some cases (Fig. 6c and d).

On the other hand, the experiences carried out in laboratory and results obtained have been employed to compute the polar shock curve and evaluate in this way the interest of this method. For each recorded blow and the first-round trip cycle (t_0 to $t_0 + 2L/c$, the shock polar curve of each material has been obtained and presented in Fig. 7a. Here, the polar curve of penetrometer rod is also plotted.

Moreover, to evaluate the sensitivity of Aussedat (1970)'s method, supplementary tests have been carried out on different natural soil samples: marlaceous clay, Allier sand (low and high density) and Fontainebleau sand. The results obtained are presented simultaneously with those achieved on sandy clay and sand samples (Fig. 7b). From presented curves (Fig. 7), the good agreement can be observed as well as repeatability of each analysed blow and its sensitivity to the type of material. Furthermore, as can be expected, the mechanical impedance (Z) obtained for rigid materials (steel and concrete) is higher than those obtained for other soil materials (Fig. 7a).

Additionally, a summary of results obtained from the interpretation of each shock polar curve achieved on each material is provided in Table 1. Here, the maximum values of force and velocity for incident (F_i , v_i), reflected (F_r , v_r) and transmitted waves (F_T , v_T) are presented. For each material, the average of mechanical impedance (Z_s), compressional wave velocity c_p and equivalent strain ϵ_p (Eqs. (11) and (12)) has been calculated assuming the linear elasticity for each tested material.

It can be noted that the obtained values of the compressional wave velocity are in good agreement with those found in the literature: 2800–3600 m/s for concrete, 3500–6000 m/s for wood, 1200–3000 m/s for marlaceous clay and 200–2200 m/s for dry/wet sands. In this way, the method proposed by Aussedat (1970) to evaluate the

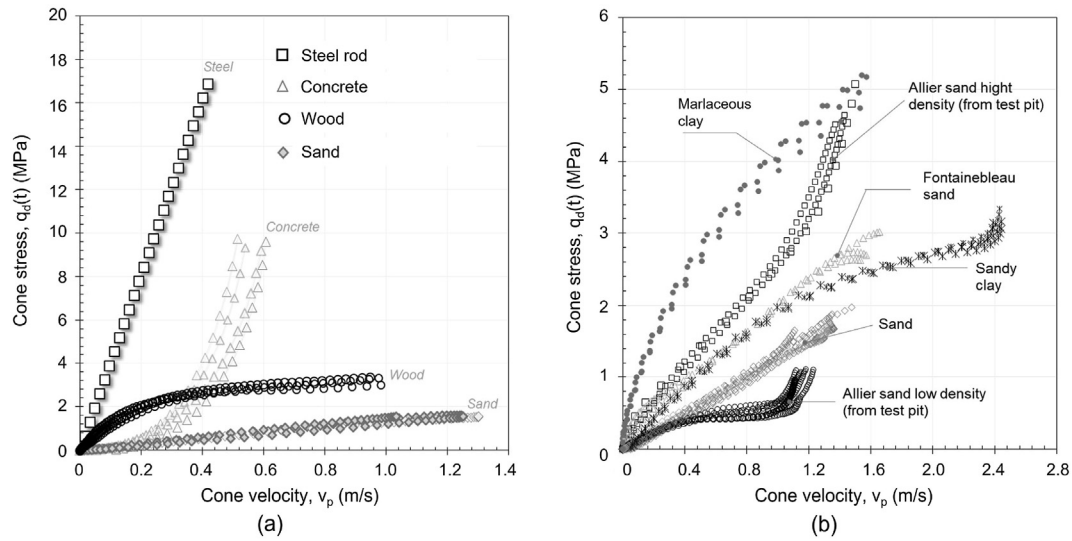


Fig. 7. Experimental shock polar curves obtained in the laboratory: (a) Comparison for different materials (concrete, clean sand, wood and steel rods), and (b) Comparison for various types of soils (compacted clayey sand, Fontainebleau sand and Allier compacted and loose sand).

Table 1
Experimental results of mechanical impedance and wave velocity assessment obtained from the polar shock curves for different materials and some recorded blows (Fig. 7).

Material	Density (kg/m ³)	Number of blows	F_r (kN)	F_g (kN)	v_r (m/s)	v_g (m/s)	σ_T (MPa)	v_t (m/s)	Z_s ((kN s)/m)	c_p (m/s)	ϵ_p (10 ⁻⁴)
Concrete	2400	10	2.35 ± 0.27	-1.45 ± 0.23	0.38 ± 0.044	-0.23 ± 0.037	4.57 ± 0.33	0.61 ± 0.08	1.48 ± 0.18	3153 ± 287	1.97 ± 0.438
Wood (Douglas fir)	530	10	5.56 ± 1.07	-4.73 ± 0.92	0.89 ± 0.17	-0.76 ± 0.15	4.12 ± 0.75	1.65 ± 0.32	0.5 ± 0.021	4714 ± 201	3.52 ± 0.745
Clean sand	1650	5	3.55 ± 0.28	-3.06 ± 0.25	0.57 ± 0.045	-0.49 ± 0.04	1.24 ± 0.104	1.06 ± 0.085	0.46 ± 0.02	713 ± 32	14.9 ± 1.53
Sandy clay	1750	10	7.91 ± 1.06	-7.05 ± 0.96	1.27 ± 0.17	-1.12 ± 0.15	2.39 ± 0.28	2.39 ± 0.32	0.39 ± 0.028	563 ± 41	42.8 ± 7.47
Marlaceous clay	2000	5	10.07 ± 0.17	-5.22 ± 0.08	1.62 ± 0.027	-0.84 ± 0.013	12.46 ± 0.396	2.45 ± 0.035	1.97 ± 0.05	2489 ± 63	9.86 ± 0.248
Low-density Allier sand	1450	10	3.93 ± 0.52	-3.61 ± 0.5	0.63 ± 0.083	-0.58 ± 0.08	0.83 ± 0.213	1.21 ± 0.163	0.27 ± 0.069	477 ± 122	27.5 ± 9.95
High-density Allier sand	1730	10	9.9 ± 1.28	-8.42 ± 1.16	1.59 ± 0.2	-1.35 ± 0.187	7.36 ± 0.803	2.94 ± 0.391	0.51 ± 0.045	1454 ± 129	20.5 ± 4.39
Fontainebleau sand	1540	10	5.57 ± 1	-4.89 ± 0.87	0.89 ± 0.161	-0.78 ± 0.14	3.41 ± 0.734	1.68 ± 0.3	0.41 ± 0.039	1319 ± 126	12.8 ± 2.45

mechanical impedance (Z_s) as well the wave velocity of soils seem to be a reliable and interesting means to characterise shallow soils.

3.2. Interpretation of DCLT curves

Besides applying the Aussedat (1970)'s method, a simple analytical method was proposed to analyse DCLT curves obtained during penetrometer driving, as shown in Fig. 8, based on simplified pile model (Benz Navarrete, 2009; Benz Navarrete et al., 2013, 2014; Escobar Valencia, 2015; Escobar Valencia et al., 2016b).

The experimental DCLT curves can be separated into three phases (Fig. 8a): full dynamic penetration, plastic shear penetration and unloading/reloading cycles. Full dynamic penetration is mainly inertial and penetration rate dependent, while plastic shear penetration is penetration rate and displacement dependent. The unloading/reloading cycle, which follows the moment when the rate penetration becomes zero (at this moment, represented by the point A in Fig. 8, the energy to penetrate the soil is not enough), is mainly elastic displacement dependent.

The DCLT is modelled as a simplistic elasto-viscoplastic model (Fig. 8a). Here, the total soil resistance $q_d(t)$ is modelled with both viscous dynamic (q_{dyn}) and pseudo-static (q_s) components (Eq. (13)). The total soil resistance is thus the sum of the spring reaction (q_s) and the radiation dashpot reaction (q_{dyn}) (Salgado et al., 2015). These two

components can be separated from each DCLT curve. Pseudo-static resistance q_s is displacement dependent and then independent of penetration rate. This is modelled by an elastic perfectly plastic law and determined experimentally when average penetration rate is zero (Eq. (14)). Knowing pseudo-static resistance value, viscous dynamic resistance (q_{dyn}) is determined from dynamic loading curves as the average resistance mobilised in the penetration interval between elastic settlement s_e and maximum measured plastic penetration s_p once pseudo-static resistance is subtracted (Eq. (15)).

$$q_d(t) = q_s + q_{dyn} \quad (13)$$

$$q_s = q_d(t_A) \forall t = t_A \text{ when } v_p(t_A) \approx 0 \text{ and } s_p(t_A) = s_p \quad (14)$$

$$q_{dyn} = \frac{1}{s_p - s_e} \int_{s_e}^{s_p} [q_d(t) - q_s] ds \quad (15)$$

Viscous dynamic resistance q_{dyn} is often explained by static resistance q_s , penetration rate $v_p(t)$ as well as by means of damping coefficient (McVay and Kuo, 1999; Charue, 2004; Hölscher et al., 2012). In this work, although interesting and important, the establishment of the damping coefficient is not discussed.

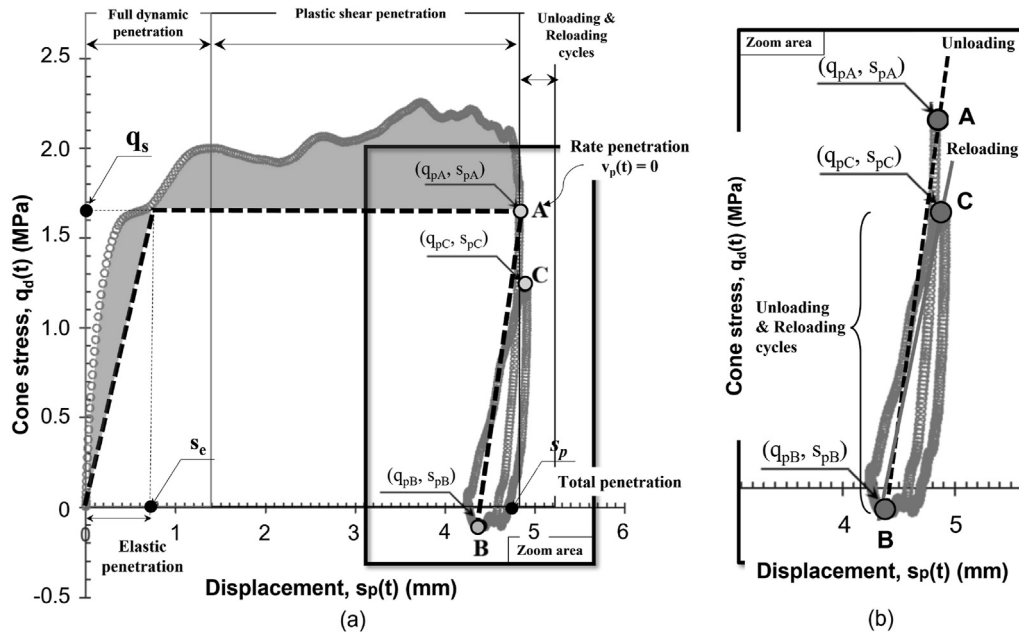


Fig. 8. Interpretation of DCLT curve based on the simple Smith (1960)'s pile model: (a) General model represented by an elasto-viscoplastic model, and (b) Unloading/reloading zoom area.

From unloading and reloading cycles (slopes AB and BC, respectively, in Fig. 8b), dynamic elastic modulus E_{p3} can be determined. Once the maximum plastic penetration s_p is reached, the soil and penetrometer vibrate together in a pseudo-elastic steady state. Here, two moduli are defined: unloading modulus E_{p3}^d and reloading modulus E_{p3}^r (Eq. (16)). Indeed, supposing that the cone penetrometer is a small circular plate embedded in a semi-infinite elastic medium, E_{p3}^d and E_{p3}^r values can be calculated from Boussinesq and Mindlin approaches (Arbaoui et al., 2006; Ali et al., 2008, 2009, 2009; Reiffsteck et al., 2008, 2009, 2019).

$$\begin{aligned} E_{p3}^d &= (1 - \nu^2) \left(\frac{q_{pA} - q_{pB}}{s_{pA} - s_{pB}} \right) \frac{\pi d_p^2}{4} \frac{1}{k_M} \\ E_{p3}^r &= (1 - \nu^2) \left(\frac{q_{pA} - q_{pB}}{s_{pA} - s_{pB}} \right) \frac{\pi d_p^2}{4} \frac{1}{k_M} \end{aligned} \quad (16)$$

where ν is the Poisson's ratio of the soil, d_p is the cone diameter, and k_M is the embedding Mindlin's coefficient.

To summarize, in practice, at the end of the dynamic penetration test according to the method presented, the following log profiles were produced: dynamic and pseudo-static cone resistance, unloading and reloading moduli, and compressional wave velocity. Shear wave velocity can be also determined by assuming the Poisson's ratio of the soil. As previously stated, considering dynamic compression as well as undrained condition, Poisson's ratio will be close to 0.5.

3.3. Laboratory tests in a sand fill

A second experiment was carried out in an experimental sand pit to evaluate the reliability of the measurements, especially the soil resistance obtained from the DCLT curve (Fig. 9).

The results are compared with those obtained, firstly, with a cone penetration test (CPT) (Gouda) providing cone resistance q_c , and secondly, with dynamic penetrometer P.A.N.D.A providing the dynamic cone resistance q_d obtained through modified Dutch

formula (Gourvès, 1991; Gourvès and Barjot, 1995; Langton, 1999). In this way, total soil resistance $q_d(t)$ (Eq. (13)) is compared with dynamic cone resistance q_d (from P.A.N.D.A) while pseudo-static resistance q_s (Eq. (14)) is compared with CPT results (q_c).

This experiment aims also to evaluate the relevance and the adaptability of the new method to obtain DCLT curves in different conditions, more precisely, at different depths, up to 3.4 m, with different rod lengths and in a same material compacted at different degrees.

As shown in Fig. 9, the external dimensions of pit are 4 m × 2.1 m × 2.9 m, and the filling material is an alluvial sand (from the Allier river, central France). A summary of the general characteristics as well as the location of each test are shown in Fig. 9a. The filler sand was deposited arbitrary in two layers (Fig. 9b). The loose-density lower layer of 2 m thick was deposited by pluviation, at low drop height with no mechanical compaction. The upper layer of 1.45 m thick was compacted with a vibrator plate compactor in 0.2 m thick layers.

Conventional DPT (P.A.N.D.A.) was carried out close to the current instrumented DPT (Fig. 9b). The tests were performed at 60 cm from each other and 60 cm from the pit edges, in order to reduce the effects of the boundary conditions considering a ratio between influence area of the test and the cone diameter at least of 50 (Schnaid and Houlsby, 1991; Bolton and Gui, 1993; Balachowski and Kurek, 2008; Wachiraporn et al., 2018). To avoid the skin friction along the rods, the tests were conducted with an overflowing cone of 4 cm² in cross-section (22.6 mm in diameter). In addition, as the rod length is 500 mm, DPT tests have been carried out with 2–4 rods within the top layer and 4–8 rods for the case of the bottom layer. As the test progresses in depth, rods were added and strongly screwed together without any additional connectors to ensure continuity and homogeneity of rod string.

Concerning the proposed instrumented DPT, three measurements of the DCLT curve were carried out at approximately every stage of 0.2 m between the depths of 0.3 m and 3.2 m. A total of 45 measurements were recorded. Some examples of DCLT curves are presented in Fig. 10. From each curve, total ($q_d(t)$) and pseudo-static (q_s) soil resistances are obtained. The mean values (grey triangles

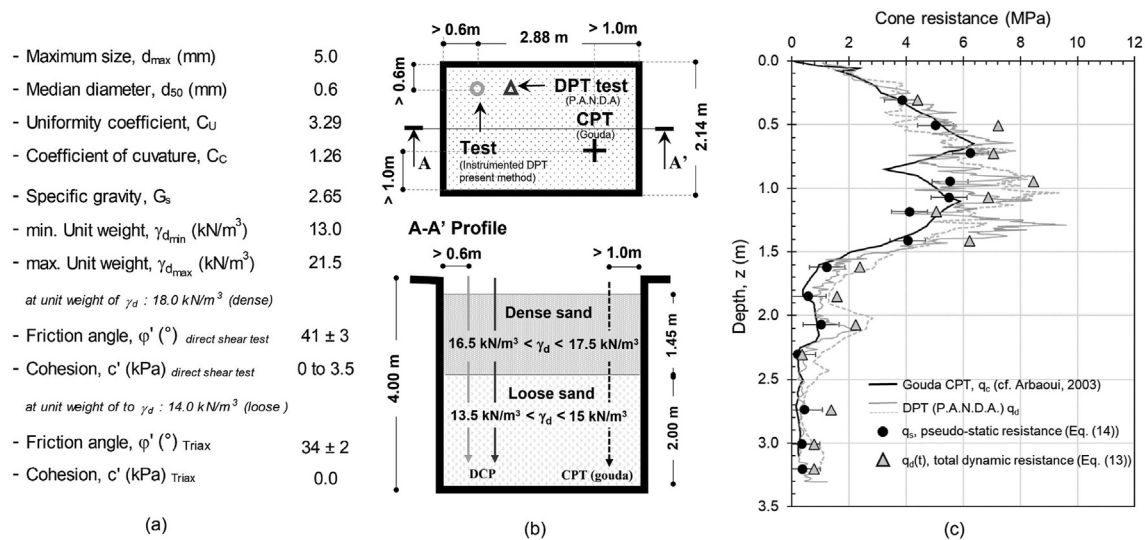


Fig. 9. Experimental results obtained in a laboratory sand pit fill: (a) Allier sand properties; (b) Diagram of experimental pit filled with Allier sand in two different layers, general view of penetration test position; and (c) Cone resistance profiles: dynamic cone resistance q_d obtained with conventional DPT (P.A.N.D.A.), static cone resistance q_c obtained with a CPT and q_s and $q_d(t)$ (pseudo-static and total soil resistances) obtained from DCLT curves performed at different depths through the present method.

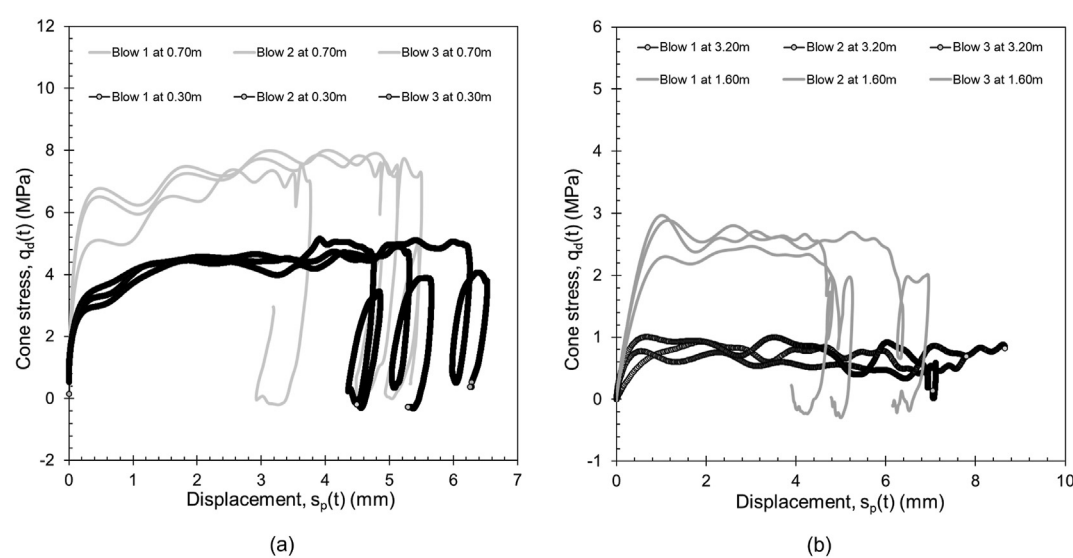


Fig. 10. Example of DCLT curves obtained in a laboratory sand pit fill for 3 consecutive blows at different depths: (a) In the upper layer at 0.3 m and 0.7 m depths, and (b) In the bottom layer at 1.6 m and 3.2 m depths.

Table 2 Comparison of the mean value of cone resistances obtained with the instrumented DPT and conventional methods (CPT and DPT) for the two layers of the sand fill pit.

Layer	Instrumented DPT (P.A.N.D.A. 3)				q_c (MPa) from CPT test (Gouda)		q_d (MPa) from conventional DPT	
	Pseudo-static resistance, q_s (MPa) (Eq. (14))		Total soil resistance, $q_d(t)$ (MPa) (Eq. (13))		Mean value	Standard deviation	Mean value	Standard deviation
	Mean value	Standard deviation	Mean value	Standard deviation				
Upper	4.36	1.59	5.72	1.81	4.26	1.35	5.53	1.69
Lower	0.5	0.29	1.1	0.65	0.53	0.4	1.01	0.71

and black circles) of the three consecutive measurements at each stage are plotted in Fig. 9c. The logs of the dynamic (q_d) and static (q_c) cone resistances obtained respectively from conventional DPT (P.A.N.D.A.) using the Dutch driving formula and the CPT (Gouda) are also plotted (Fig. 9c).

The results of the cone resistances obtained by means of the proposed instrumented DPT show a good agreement (Fig. 9c) with those obtained with conventional devices (Table 2). Indeed, about pseudo-static and static (CPT) cone resistances, the mean values as well as the standard deviations for two layers are very similar, as

shown by Odebrecht et al. (2005), and Schnaid et al. (2007, 2009, 2017). Regarding the total ($q_d(t)$) and dynamic (q_d) cone resistances, the values obtained from dynamic load curves are slightly higher than the values obtained with the driving formulae.

Furthermore, in Fig. 10, some DCLT curves for successive blows are presented. These curves were smoothed using a low-pass FIR filter (Hamming windows) with a cut-off frequency varying from 900 Hz to 300 Hz to attenuate the natural modes of rods. A good repeatability of the curves for each layer can be observed as well as a sensitivity to the sand compaction degree. In both cases, elastic deformation, plasticity threshold and unloading/reloading cycles can be identified. Nevertheless, due to the low resistance of the lower sand layer, unloading/reloading cycles after the main penetration were not observed. In this case, when very soft soils are tested, it seems more appropriate to adapt the driving energy to the minimum.

4. Full-scale tests

A final test was carried out to assess the feasibility of the proposed method in the field. The test site is located in the vicinity of Castelló d'Empúries in the Alt Empordà, close to the Costa Brava, north of Barcelona, Spain. This is an alluvial plain mostly formed by deposits of the Fluvià and Muga rivers. In this site, the Holocene deposits reach a thickness of about 20–30 m in the area, with alternating sand dominated deposits and silt-clay deposits. At the surface of this site, a very compacted backfill of approximately 1.5 m thick was built (Perez et al., 2013; Arroyo et al., 2015). The groundwater table was located at a depth of 2.4 m below the ground surface.

Concerning the measurements performed with the instrumented DPT, a total of six soundings were conducted. These were dropped to an average depth of 7.2 m, while minimal and maximal depth reached were 5.7 m and 10.1 m, respectively. Steel rods of 500 mm in length and 14 mm in diameter, screwed tightly together during probing, were used. No additional connectors between two rods were employed.

To reduce the skin friction along the rods, overflow cones of 4 cm² in cross-section has been used. Because the ratio between cone and rod diameters is greater than 1.6, the skin friction can be significantly reduced. Indeed, the skin friction was checked each 1 m of driving by means of the torque measurement. This was

negligible in all cases, which was confirmed additionally by using the methods developed in dynamic pile load test to identify the shaft forces (Rausche, 1970; Goble et al., 1980; Goble and Aboumatar, 1992).

Each test was driven by variable driving energy using a hand hammer, adapting the power of blow to the soil resistance. Stress, acceleration, and displacement measurements were performed continuously blow by blow for all tests. In total, 5932 blows were recorded, which represents an average of 135 blows/m. In this way, a dynamic cone penetration curve was obtained almost every 7.5 mm of penetration.

The results obtained for each parameter are plotted as a function of the depth in Fig. 11. Here, the logs of total soil resistance $q_d(t)$, pseudo-static cone resistance q_s , compressional (c_p) and shear (c_s) wave velocities, unloading (E_{p3}^d) and reloading (E_{p3}^r) penetrometric moduli are presented. Considering undrained condition of soil and dynamic loading, Poisson's ratio of 0.49 was employed.

The average value for each parameter is also presented (grey continuous line) as a function of the depth. The dotted horizontal grey line indicates the groundwater table (at 2.4 m depth). Thus, the information available and the resulting profiles can be used to easily identify two shallow layers: a sandy gravel fill up to 1.2 m deep, followed by silty clay and soft sandy clay.

As different geotechnical tests (CPT, pressurometer (PMT), seismic dilatometer (sDMT), multi-channel analysis of surface waves (MASW), etc.) have been carried out in previous investigations (Perez et al., 2013; Arroyo et al., 2015), a comparison of the available values for CPTu's cone resistance as well as S-wave velocities (sDMT and MASW) measured on site with the static cone resistance and S-wave velocity obtained with the instrumented DPT is presented (Fig. 12). Although for the first meter (compacted backfill layer), a difference is observed in terms of cone resistance, it can be noted that the obtained values in deeper layer, either for cone resistances or for wave velocities, are in good agreement with the values measured previously on this site and published by Perez et al. (2013). The differences observed, especially in near surface and at 5.4 m depth, can be explained by the soil heterogeneity and the uncertainty of data provided by each method compared here (geometry, inversion method, observation scale, representative elementary volume, vertical resolution, wave damping in rods, etc.). Finally, compressional and shear wave velocities under the groundwater table must be considered carefully, even though the

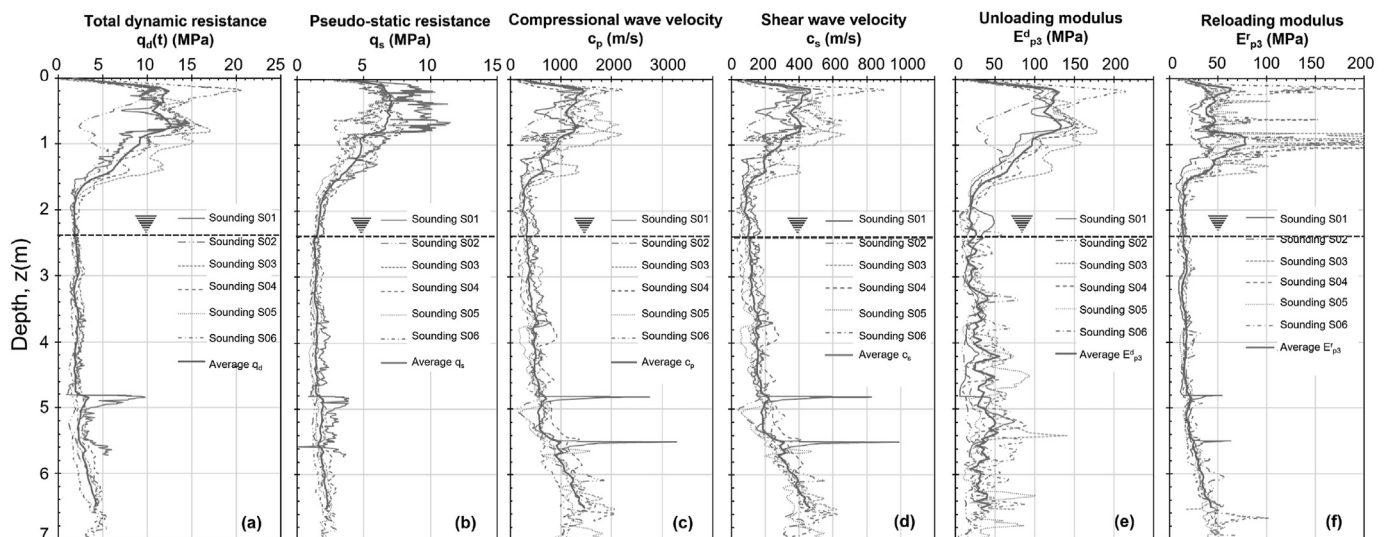


Fig. 11. Results of experimental tests performed in the vicinity of Castelló d'Empúries (Spain): $\log_{10}z$ curves of (a) total soil resistance $q_d(t)$, (b) pseudo-static cone resistance q_s , (c) compressional wave velocity c_p , (d) shear wave velocity c_s , (e) unloading penetrometric modulus E_{p3}^d , and (f) reloading penetrometric modulus E_{p3}^r .

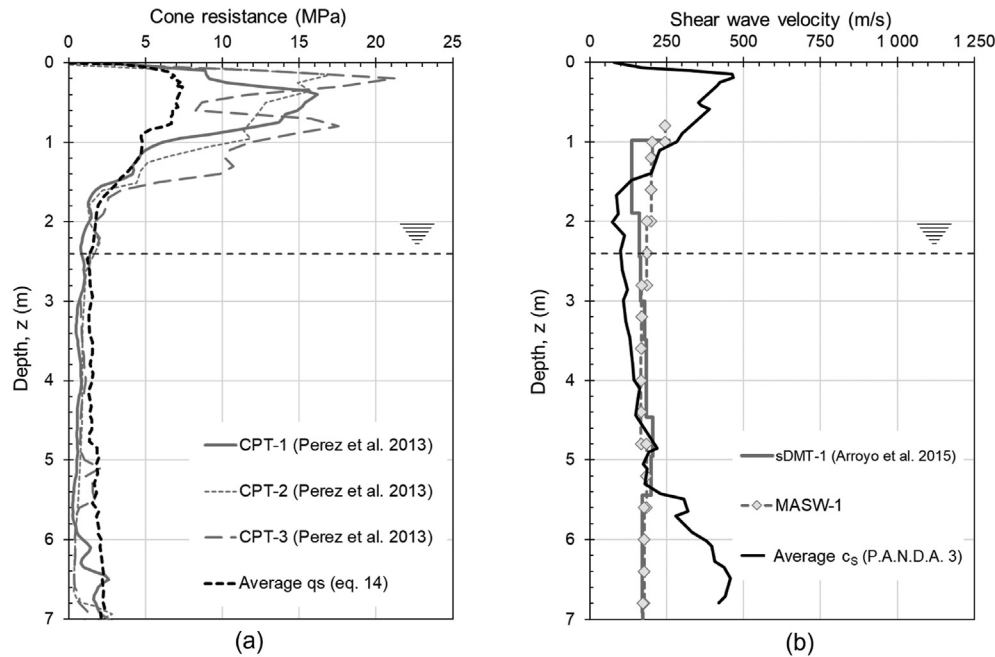


Fig. 12. Results of experimental tests performed in the vicinity of Castelló d'Empúries (Spain): comparison of (a) the cone resistances and (b) shear wave velocity measured from the new instrumented DPT with previous conventional measurements carried out on the same site (cf. [Perez et al., 2013](#); [Arroyo et al., 2015](#)).

results obtained seem in agreement with the values reported in the literature.

5. Conclusions

DPTs are widely used around the world and currently provide a single failure parameter whose interpretation is still largely empirical. Several authors proposed to improve the interpretation of the DPT by using the wave equation. However, none of these works have been implemented in practice to obtain in situ soil stress and strain relationship necessary for the most current geotechnical problems.

In this work, a lightweight dynamic variable energy penetrometer has been instrumented to measure the strain $\epsilon(x, t)$, acceleration $a(x, t)$ and displacement $s(t)$ variations caused within the rods by the compressional wave created immediately after each hammer blow and during penetrometer driving. By using a wave decoupling and reconstruction method, it has been possible to obtain the DCLT curve of the soil at each blow.

As demonstrated by a series of tests on different materials, the resulting DCLT curve is reproducible, sensitive, and reliable to the test conditions as well as to the soil conditions. Moreover, the implementation of the method based on a linear viscoelastic model and the [Smith \(1960\)](#) approach makes it possible to compute total, dynamic and pseudo-static soil resistances as well as the deformability moduli from DCLT curve. Finally, the application of the method proposed by [Aussedat \(1970\)](#) makes it possible to determine the soil impedance or shock polar curve, from which the soil compressional wave velocity can be calculated.

It is important to note that the test proposed here, manually driven with adapted energy, is not affected by the subsequent hammer rebounds as noted in previous SPT energy measurement works. The technical feasibility of the method as well as the reliability of the results has been proved in situ by a series of tests with continuous recordings up to a depth of 7 m.

Considering that for one linear meter of sounding, almost 200 hammer blows are provided and that from each curve, a series of

parameters is produced, the amount of information collected during a field test is highly significant and in the long-term will facilitate implementation of statistical analysis methods for the data analysis.

The method proposed here is not P.A.N.D.A. specific and can be applied to the other DPTs by being vigilant to avoid the skin friction along the rods. This can be achieved by using cones with larger diameters than those of the rods or most traditional techniques as mud injection or outer casing, as described in [ISO-22476-2 \(2005\)](#). Anyway, if skin friction is present, back analysis or fitting methods commonly used in pile loading test ([Rausche, 1970](#); [Rausche et al., 1972](#); [Goble et al., 1980](#); [Loukidis et al., 2008](#); [Salgado et al., 2015, 2017, 2017](#); [Poganski et al., 2016, 2017](#)) can be adapted to obtain cone response.

Also, it should be noted that if the penetrometer driving energy is too high for low-consistency and saturated soils or for the tests performed below the groundwater table, the assessment of compressional waves obtained through the present method can be highly affected. In such cases and according to the current state of knowledge regarding dynamic signal processing, the values obtained are likely to be higher and should be carefully considered.

Despite the results obtained, the soil behaviour subjected to cone penetration remains poorly understood. Indeed, this is a non-homogeneous loading test, and given its nonlinearity, the soil behaviour after blow is complex. This is why interpretation of the DCLT curve is a complex matter and should be the subject of future studies to improve its understanding, and to develop methods in order to estimate intrinsic soil parameters governing stress-strain behaviour under dynamic penetration.

Declaration of competing interest

The authors declare that they have no known competing financial interests or personal relationships that could have appeared to influence the work reported in this paper.

References

- Abbott, M.B., 1966. An introduction to the method of characteristics. In: *Finite Difference Methods in Financial Engineering: A Partial Differential Equation Approach*. Cambridge University Press, Cambridge, UK, pp. 47–59.
- Aboumatar, H., Goble, G.G., 1997. SPT dynamic analysis and measurements. *J. Geotech. Geoenviron. Eng.* 123, 921–928.
- Ali, H., Reiffsteck, P., Bacconnet, C., Gourvès, R., Baguelin, F., van de Graaf, H., 2008. Facteurs d'influence de l'essai de chargement de pointe. Nantes, France. In: *Journées Natl. Géotechnique Géologie l'Ingénieur JNGG'08*, pp. 467–474 (in French).
- Ali, H., Reiffsteck, P., van de Graaf, H., van de Stoel, A.E.C., Gourvès, R., Bacconnet, C., et al., 2009. Essai de chargement de pointe: facteurs d'influence et détermination de modules de déformation. In: *Proceedings of the 17th International Conference on Soil Mechanics and Geotechnical Engineering*, vol. 2, pp. 985–988 (in French).
- Arbaoui, H., Gourvès, R., Bressollette, P., Bodé, L., 2006. Mesure de la déformabilité des sols in situ à l'aide d'un essai de chargement statique d'une pointe pénétrométrique. *Can. Geotech. J.* 43, 355–369 (in French).
- Arroyo, M., Pineda, J.A., Sau, N., Devicenzi, M., Perez, N., 2015. Sample quality examination on silty soils. In: *ICE Proceedings of the 16th ECSMGE Geotechnical Engineering for Infrastructure and Development*, vol. 6, pp. 2873–2878.
- Aussedat, G., 1970. Sollicitations rapides des sols. PhD Thesis. University of Grenoble, Grenoble, France (in French).
- Balachowski, L., Kurek, N., 2008. Influence of boundary conditions in penetration testing. *Arch. Civ. Eng.* 54 (4), 653–668.
- Batilas, A., Pelekis, P.G., Roussos, P., Athanasopoulos, G.A., 2016. SPT energy measurements: manual vs. automatic hammer release. *Geotech. Geol. Eng.* 35, 879–888.
- Benz Navarrete, M.A., 2009. Mesures dynamiques lors du battage du pénétromètre Panda 2. PhD Thesis. University of Clermont-Auvergne, Clermont-Ferrand, France (in French).
- Benz Navarrete, M.A., Escobar Valencia, E.J., Gourvès, R., Haddani, Y., Breul, P., Bacconnet, C., 2013. Mesures dynamiques lors du battage pénétrométrique – Détermination de la courbe charge-enfoncement dynamique en pointe. In: *Proceedings of the 18th International Conference on Soil Mechanics and Geotechnical Engineering*, vol. 1, pp. 499–502. Paris, France.
- Benz Navarrete, M.A., Escobar Valencia, E.J., Haddani, Y., Gourvès, R., Costa D'Aguiar, S., Calon, N., 2014. Determination of soil dynamic parameters by the Panda 3®: railways platform case. In: *Proceedings of the 2nd International Conference on Railway Technology: Research, Development and Maintenance*, vol. 56, pp. 1–15.
- Bolton, M.D., Gui, M.W., 1993. The study of relative density and Boundary conditions effects for cone penetration test in centrifuge. In: *Technical Report No. CUED/D-SOILS/TR256*. Cambridge University, Cambridge, England.
- Breul, P., Benz Navarrete, M.A., Gourvès, R., Saussine, G., 2009. Penetration test modelling in a coarse granular medium. In: *Proceedings of the 6th International Conference on Micromechanics of Granular Media*, vol. 1145, pp. 173–176. Powders and Grains.
- Bussac, M.N., Collet, P., Gary, G., Othman, R., 2002. An optimisation method for separating and rebuilding one-dimensional dispersive waves from multi-point measurements. Application to elastic or viscoelastic bars. *J. Mech. Phys. Solid.* 50 (2), 321–349.
- Butler, J., Caliendo, J., Goble, G.G., 1998. Comparison of SPT energy measurement methods. In: *Proceedings of the 1st International Conference on Site Characterization*, vol. 2, pp. 901–905.
- Byun, Y.H., Lee, J.S., 2013. Instrumented dynamic cone penetrometer corrected with transferred energy into a cone tip: a laboratory study. *Geotech. Test J.* 36 (4), 533–542.
- Carlsson, J., Sundin, K.G., Lundberg, B., 1990. A method for determination of in-hole dynamic force-penetration data from two-point strain measurement on a percussive drill rod. *Int. J. Rock Mech. Min. Sci. Geomech. Abstr.* 27 (6), 553–558.
- Casem, D.T., Fourney, W., Chang, P., 2003. Wave separation in viscoelastic pressure bar using single point measurements of strain and velocity. *Polym. Test.* 22 (2), 155–164.
- Charue, N., 2004. Loading Rate Effects on Pile Load-Displacement Behaviour Derived from Back-Analysis of Two Load Testing Procedures. PhD Thesis. University of Louvain, Louvain-la-Neuve, Belgium.
- Chen, C., 1991. Energy Measurements during the Standard Penetration Test. MS Thesis. University of Colorado, Boulder, Colorado, USA.
- Eiksund, G., Nordal, S., 1996. Dynamic model pile testing with pore pressure measurements. *Proceedings of the 5th International Conference of Applied Stress-Wave Theory to Piles*, pp. 581–588.
- Escobar Valencia, E.J., 2015. Mise au point et exploitation d'une nouvelle technique pour la reconnaissance des sols : le PANDA 3. PhD Thesis. University of Clermont-Auvergne, Clermont-Ferrand, France (in French).
- Escobar Valencia, E.J., Benz Navarrete, M.A., Gourvès, R., Breul, P., 2013. Dynamic cone penetration tests in granular media: determination of the tip's dynamic load-penetration curve. In: *Proceedings of the 7th International Conference on Micromechanics of Granular Media*, vol. 1542, pp. 389–392. Powder and Grains.
- Escobar Valencia, E.J., Benz Navarrete, M.A., Gourvès, R., Breul, P., Chevalier, B., 2016a. In-situ determination of soil deformation modulus and the wave velocity parameters using the Panda 3®. In: *Proceedings of the 5th Geotechnical on Geotechnical and Geophysical Site Characterization (ISC'5)*, vol. 1, pp. 279–284.
- Escobar Valencia, E.J., Benz Navarrete, M.A., Gourvès, R., Haddani, Y., Breul, P., Chevalier, B., 2016b. Dynamic characterization of the supporting layers in railway tracks using the dynamic penetrometer Panda 3®. *Procedia Eng.* 143, 1024–1033.
- Farrar, J.A., 1998. Summary of Standard penetration test (SPT) energy measurement experience. In: *Proceedings of the 1st International Conference on Site Characterization*, vol. 1. ISC'98, pp. 919–926.
- Farrar, J.A., Nickell, J., Allen, M.G., Goble, G.G., Berger, J., 1998. Energy loss in long rod penetration testing - terminus dam liquefaction investigation. In: *Proceedings of the ASCE Specialty Conference on Geotechnical Earthquake Engineering and Soil Dynamics III*, vol. 75, pp. 554–567.
- Goble, G.G., Aboumatar, H., 1992. Determination of wave equation soil constants from the standard penetration test. In: *Proceedings of the 4th International Conference of Applied Stress-Wave Theory to Piles*, pp. 99–103.
- Goble, G.G., Aboumatar, H., 1994. Dynamic Measurements on Penetrometers for Determination of Foundation Design. University of Colorado, Boulder, Colorado, USA. Technical Report No. CDOH-DTD-R-94-12.
- Goble, G.G., Likins, G.E., Rausche, F., 1975. Bearing capacity of piles from dynamic measurements. Case Western Reserve University, Cleveland, Ohio, USA. Technical Report No. OHIO-DOT-05-75.
- Goble, G.G., Rausche, F., Linkins, G.E., 1980. The analysis of pile driving - a State-of-the-art. In: *Proceedings of the International Seminar on the Application of Stress-Wave Theory on Piles*, pp. 131–161.
- Gonin, H., 1979. Réflexions sur le battage des pieux. *Rev. Fr. Geotech.* 9, 41–50 (in French).
- Gonin, H., 1996. Du pénétromètre dynamique au battage des pieux. *Rev. Fr. Geotech.* 76, 35–44 (in French).
- Gonin, H., 1999. La formule des Hollandais ou le conformisme dans l'enseignement. *Rev. Fr. Geotech.* 87, 35–42 (in French).
- Gourvès, R., 1991. Le PANDA : pénétromètre dynamique léger à énergie variable pour la reconnaissance des sols. University of Clermont-Auvergne, Clermont-Ferrand, France (in French).
- Gourvès, R., Barjot, R., 1995. Le pénétromètre dynamique léger PANDA. In: *Proceedings of 11ème Congrès Eur. Mécanique des sols des Trav. Fond.*, pp. 83–88.
- Holeyman, A., 1992. Technology of pile dynamic testing. In: *Proceedings of the 4th International Conference of Applied Stress-Wave Theory to Piles*, pp. 195–215.
- Hölscher, P., Brassinga, H., Brown, M., Middendorp, P., Profttlich, M., van Tol, F., 2012. Rapid Load Testing on Piles Interpretation Guidelines, first ed. CRC Press, Boca Raton, Florida, USA.
- Hussein, M.H., Goble, G.G., 2004. A brief history of the application of stress-wave theory to piles. In: *Geotechnical Special Publication*, vol. 125. American Society of Civil Engineers (ASCE), pp. 186–201.
- Isaacs, D.V., 1931. Reinforced concrete pile formulae. *J. Inst. Eng. Aust.* 12, 312–323.
- Iskander, M., Bless, S., Omidvar, M., 2015. Rapid Penetration into Granular Media: Visualizing the Fundamental Physics of Rapid Earth Penetration. Elsevier.
- ISO-22476-2, 2005. Geotechnical Investigation and Testing — Field Testing — Part 2: Dynamic Probing. European Standard, Brussels, Belgium.
- Jung, B., Park, Y., Park, Y.S., 2006. Longitudinal acceleration wave decomposition in time domain with single point axial strain and acceleration measurements. In: *Proceedings of the 8th International Conference on Motion and Vibration Control. MOVIC 2006*, pp. 1–6.
- Karlsson, L.G., Lundberg, B., Sundin, K.G., 1989. Experimental study of a percussive process for rock fragmentation. *Int. J. Rock Mech. Min. Sci.* 26 (1), 45–50.
- Kelevisius, K., Žaržojus, G., 2016. Initial DPSH soil test results with accelerometer installed in the probe cone. In: *Proceedings of the 13th Baltic Sea Region Geotechnical Conference*, pp. 118–121.
- Kianirad, E., Gamache, R., Brady, D., Alshawabkeh, A., 2011. Equivalent quasi-static estimation of dynamic penetration force for near surface soil characterization. In: *Proceedings of Geo-Frontiers Congress 2011*. American Society of Civil Engineers (ASCE), pp. 2325–2334.
- Kotroc, K., Mouazen, A.M., Kerényi, G., 2016. Numerical simulation of soil–cone penetrometer interaction using discrete element method. *Comput. Electron. Agric.* 125, 63–73.
- Langton, D.D., 1999. The Panda lightweight penetrometer for soil investigation and monitoring material compaction. *Gr. Eng.* 32, 33–37.
- Liang, R.Y., Sheng, Y., 1993. Wave equation parameters from driven-rod test. *J. Geotech. Eng.* 119 (6), 1037–1057.
- Lodygowski, T., Rusinek, A., 2014. Constitutive Relations under Impact Loadings: Experiments, Theoretical and Numerical Aspects. Springer, Heidelberg, Germany.
- Loukidis, D., Salgado, R., Abou-Jaoude, G., 2008. Assessment of Axially-Loaded Pile Dynamic Design Methods and Review of INDOT Axially-Loaded Pile Design Procedure. Purdue University, West Lafayette, Indiana, USA. Technical Report No. FHWA/IN/JTRP-2008/6.
- Lowery, L.L., Finley, J.R., Hirsch, T.J., 1968. A comparison of dynamic pile driving formulas with the wave equation. Texas Transportation Institute, Texas A&M University, Texas, USA. Technical Report No. 33-12.
- Lundberg, B., Henchoz, A., 1977. Analysis of elastic waves from two-point strain measurement. *Exp. Mech.* 17 (6), 213–218.
- Massarch, K.R., 2014. Cone penetration testing – a historic perspective. In: *Proceedings of the 3rd International Symposium of Cone Penetration Testing (CPT'14)*, vol. 4, pp. 97–134. KN.

- Mcvay, M.C., Kuo, C.L., 1999. Estimate Damping and Quake by Using Traditional Soil Testing. In: Technical Report No. FDOT-BB-508. University of Florida, Gainesville, Florida, USA.
- Meunier, J., 1974. Contribution à l'étude des ondes et des ondes de choc dans les sols. PhD Thesis. University of Grenoble, Grenoble, France (in French).
- Middendorp, P., Verbeek, G., 2006. 30 years of experience with the wave equation solution based on the method of characteristics. In: Proceedings of GeoCongress 2006, pp. 1–5.
- Middendorp, P., Weele, V., 1986. Application of characteristic stress wave method in offshore practice. In: Proceedings of the 3rd International Conference on Numerical Methods in Offshore Piling, vol. 1, pp. 6–18.
- Nazarian, S., Tandom, V., Crain, K., Yuan, D., 1998. Feasibility Study on Improvements to Dynamic Cone Penetrometer. University of Texas, El Paso, Texas, USA. Technical Report No. TX-97 3903-2.
- Odebrecht, E., Schnaid, F., Rocha, M., Bernardes, G., 2005. Energy efficiency for standard penetration tests. J. Geotech. Geoenviron. Eng. 131 (10), 1252–1263.
- Omidvar, M., Iskander, M., Bless, S., 2014. Response of granular media to rapid penetration. Int. J. Impact Eng. 66, 60–82.
- Omidvar, M., Malioche, J.D., Bless, S., Iskander, M., 2015. Phenomenology of rapid projectile penetration into granular soils. Int. J. Impact Eng. 85, 146–160.
- Othman, R., 2014. Comparison of three methods to separate waves in the processing of long-time Hopkinson bar experiments. Int. J. Mech. Eng. Technol. 5, 114–119.
- Oularbi, A., 1989. Applicabilité des mesures dynamiques au calcul des pieux. PhD Thesis. University of Nantes, Nantes, France (in French).
- Oularbi, A., Levacher, D., 2009. Réponse dynamique de la pointe d'un modèle de pieu dans un sol granulaire. In: Proceedings of the Coastal and Maritime Mediterranean Conference, vol. 1, pp. 49–52.
- Palacios, A., 1977. The Theory and Measurement of Energy Transfer during Standard Penetration Test Sampling. PhD Thesis. University of Florida, Gainesville, USA.
- Park, S.W., Zhou, M., 1999. Separation of elastic waves in split Hopkinson bars using one-point strain measurements. Exp. Mech. 39, 287–294.
- Perez, N., Sau, N., Devicenzi, M., Arroyo, M., Pineda, J., 2013. Pressiometric and non-pressiometric tools on a Mediterranean deltaic deposit. In: Proceedings of the 6th International Symposium on Pressuremeters (ISP6), vol. 1, pp. 44–47.
- Poganski, J., Kömle, N., Kargl, G., F. Schweiger, H., Grott, M., Spohn, T., et al., 2016. Extended pile driving model to predict the penetration of the insight/HP3 mole into the Martian soil. Space Sci. Rev. 211, 217–236.
- Poganski, J., Schweiger, H.F., Kargl, G., Kömle, N.I., 2017. DEM modelling of a dynamic penetration process on mars as a part of the NASA insight mission. Procedia Eng 175, 43–50.
- Quezada, J.C., Breul, P., Saussine, G., Radjai, F., 2014. Penetration test in coarse granular material using contact dynamics method. Comput. Geotech. 55, 248–253.
- Rausche, F., 1970. Soil Response from Dynamic Analysis and Measurements on Piles. PhD Thesis. Case Western Reserve University, Cleveland, USA.
- Rausche, F., Goble, G.G., Likins, G.E., 1985. Dynamic determination of pile capacity. J. Geotech. Eng. 111 (3), 367–383.
- Rausche, F., Goble, G.G., Moses, F., 1971. A new testing procedure for axial pile strength. In: Proceedings of Offshore Technology Conference, vol. 1, pp. 633–642.
- Rausche, F., Moses, F., Goble, G.G., 1972. Soil resistance predictions from pile dynamics. J. Soil Mech. Found Div. 98 (9), 917–937.
- Reiffsteck, P., Bacconnet, C., Gourvès, R., Goddé, E., van de Graaf, H., 2008. Determination of elastic modulus from stress controlled cone penetration test. In: Proceedings of the 3rd International Conference on Site Characteriation, vol. 1. ISC'3, pp. 1135–1138.
- Reiffsteck, P., Thorel, L., Bacconnet, C., Gourvès, R., van de Graaf, H., 2009. Measurements of soil deformation by means of cone penetrometer. Soils Found. 49 (3), 397–408.
- Ross, C.A., Nash, P.T., Friesenhahn, G.J., 1986. Pressure Waves in Soils Using a Split-Hopkinson Pressure Bar. Southwest Research Institute, San Antonio, Texas, USA. Technical Report No. ESL-TR-86-29.
- Salgado, R., Loukidis, D., Abou-Jaoude, G., Zhang, Y., 2015. The role of soil stiffness non-linearity in 1D pile driving simulations. Geotechnique 65 (3), 169–187.
- Salgado, R., Zhang, Y., Abou-Jaoude, G., Loukidis, D., Bisht, V., 2017. Pile driving formulas based on pile wave equation analyses. Comput. Geotech. 81, 307–321.
- Sanglerat, G., 1972. The penetrometer and soil exploration. In: Developments in Geotechnical Engineering, first ed. Elsevier, New York, USA.
- Schmertmann, J.H., 1979. Statics of SPT. J. Geotech. Eng. Div. 105 (GT5), 655–670.
- Schmertmann, J.H., 1978. Use the SPT to measure dynamic soil properties?—yes. But... In: Dynamic Geotechnical Testing, vol. 654 ASTM, STP, pp. 341–355.
- Schmertmann, J.H., Palacios, A., 1979. Energy dynamics of SPT. J. Geotech. Eng. Div. 105 (8), 909–926.
- Schnaid, F., Houlsby, G.T., 1991. An assessment of chamber size effects in the calibration of in situ tests in sand. Geotechnique 41 (3), 437–445.
- Schnaid, F., Lourenço, D., Odebrecht, E., 2017. Interpretation of static and dynamic penetration tests in coarse-grained soils. Géotech. Lett. 7 (2), 113–118.
- Schnaid, F., Odebrecht, E., Rocha, M., 2007. On the mechanics of dynamic penetration tests. Geomechanics Geoenviron. 2 (2), 137–146.
- Schnaid, F., Odebrecht, E., Rocha, M., Bernardes, G., 2009. Prediction of soil properties from the concepts of energy transfer in dynamic penetration tests. J. Geotech. Geoenviron. Eng. 135 (8), 1092–1100.
- Seed, H.B., Tokimatsu, K., Harder, F.L., Chung, R.M., 1985. Influence of SPT procedures in soil liquefaction resistance evaluations. J. Geotech. Eng. 111 (2), 1425–1445.
- Skempton, A.W., 1986. Standard penetration test procedures and the effects in sands of overburden pressure, relative density, particle size, ageing and over-consolidation. Geotechnique 36 (3), 425–447.
- Smith, E.A.L., 1960. Pile driving analysis by the wave equation. J. Soil Mech. Found Div. 86 (4), 35–61.
- Sy, A., Campanella, R.G., 1991. An alternative method of measuring SPT energy. In: Proceedings of the 2nd International Conferences on Recent Advances in Geotechnical Earthquake Engineering and Soil Dynamics, vol. 1, pp. 499–505.
- Tran, Q.A., Benz Navarrete, M.A., Breul, P., Chevalier, B., Moustan, P., 2019. Soil dynamic stiffness and wave velocity measurement through dynamic cone penetrometer and wave analysis. In: Proceedings of the 16th Pan-American Conference on Soil Mechanics and Geotechnical Engineering, vol. 1, pp. 401–408.
- Tran, Q.A., Chevalier, B., Benz Navarrete, M.A., Breul, P., Gourvès, R., 2017. Modeling of light dynamic cone penetration test - panda 3 ® in granular material by using 3D Discrete element method. In: Proceedings of the 8th International Conference on Micromechanics on Granular Media, vol. 140, pp. 1–4.
- Tran, Q.A., Chevalier, B., Breul, P., 2018. Spectral analysis of the response of coarse granular material to dynamic penetration test modelled with DEM. Int. J. Geosynth. Gr. Eng. 4 (22), 1–10.
- Tran, Q.A., Chevalier, B., Breul, P., 2016. Discrete modeling of penetration tests in constant velocity and impact conditions. Comput. Geotech. 71, 12–18.
- Verruijt, A., 2010. An Introduction to Soil Dynamics, 24th ed. Springer, Dordrecht, the Netherlands.
- Wachiraporn, S., Sawangsuriya, A., Sramoon, W., 2018. Effect of boundary conditions on dynamic cone penetrometer test. In: Proceedings of the 3rd World Congress on Civil, Structural, and Environmental Engineering, vol. 1, pp. 1–4.
- Widehammar, S., 2004. Stress-strain relationships for spruce wood: influence of strain rate, moisture content and loading direction. Exp. Mech. 44, 44–48.
- Žaržojus, G., Kelevisius, K., Amsiejus, J., 2013. Energy transfer measuring in dynamic probing test in layered geological strata. Procedia Eng 57, 1302–1308.
- Zhang, N., Arroyo, M., Ciantia, M.O., Gens, A., Butlanska, J., 2019. Standard penetration testing in a virtual calibration chamber. Comput. Geotech. 111, 277–289.
- Zhao, H., Gary, G., 1997. A new method for the separation of waves. Application to the SHPB technique for an unlimited duration of measurement. J. Mech. Phys. Solid. 45 (7), 1185–1202.
- Zhou, S.S., 1997. P.A.N.D.A. PhD Thesis. In: Carcterisation des sols de surface a l'aide du penetrometre dynamique léger a energie variable type. University of Clermont-Auvergne, France (in French).



Miguel Angel Benz Navarrete obtained his BSc degree in Construction Engineering from Pontifical Catholic University of Valparaíso (PUCV), Chile, in 2004, and his MSc and PhD degrees in Materials, Structures, Reliability in Civil and Mechanical Engineering from Clermont Auvergne University, Clermont Ferrand, France, in 2005 and 2009, respectively. Since 2005, he has been affiliated as a research engineer with the scientific research and technical development department of Sol Solution SAS, a geotechnical consulting company based in Riom, France. He is currently in charge of innovation, research and development department as well as technical advisor at Sol Solution company, whose main mission is to design and develop innovative solutions in the field of in situ soil characterisation, earthworks compaction control, geotechnical and geophysical surveys, and high-yield diagnostics of transport structures with low impact on soil-structure interaction. His main skills and research interests include in situ geotechnical and geophysical tests, dynamic penetrometer improvement, pile driving and stress wave theory, borehole image analysis, numerical modeling (DEM/FEM), instrumentation, signal processing and data analysis as well as development of software and in situ test databases for soil interpretation, processing, spatialization and field modeling. He has co-directed 4 PhD theses to completion and at least 30 Eng/MSc/PhD internship students in their final research dissertations with the company and different national and international universities.